Passively *Q*-switched cylindrical vector laser based on a black phosphorus saturable absorber

Zhiwen He (贺志文), **Yang Zheng** (郑 杨), **Hongyan Liu** (刘宏燕), **Mingkun Li** (李铭坤), **Hua Lu** (陆 华)*, **Heze Zhang** (张何泽), **Qingliang Feng** (冯晴亮), **and Dong Mao** (毛 东)**

MOE Key Laboratory of Material Physics and Chemistry under Extraordinary Conditions, and Shaanxi Key Laboratory of Optical Information Technology, School of Science, Northwestern Polytechnical University, Xi'an 710072, China

**Corresponding author: hualu@nwpu.edu.cn; **corresponding author: maodong@nwpu.edu.cn*

Received October 25, 2018; accepted November 29, 2018; posted online January 24, 2019

We demonstrate an all-fiber *Q*-switched cylindrical vector laser based on a black phosphorus saturable absorber and a transverse mode converter. The saturable absorber is prepared by incorporating the polyvinyl alcohol with anti-oxidized black phosphorus nanosheets exfoliated in aqueous poly(dimethyldiallyl ammonium chloride) solution. The mode converter is composed of a tapered two-mode fiber and a single-mode fiber, and it can excite switchable azimuthally and radially polarized beams by modulating the input polarization. By enhancing the pump power from 64.68 to 174.82 mW, the repetition rate of the *Q*-switched azimuthally/radially polarized laser enlarges from 16.72/19.25 to 30.71/37.82 kHz.

OCIS codes: 140.3540, 190.4400, 140.3500.
doi: 10.3788/COL201917.020004.

Attributing to the axially symmetrical distribution of polarization[1], cylindrical vector beam (CVB) exhibits a doughnut-like intensity profile, and it has been broadly applied in fields of material processing[2], particle trapping[3], plasmonic focusing[4,5], and data storage[6]. The most famous CVBs are azimuthally polarized beam (APB) and radially polarized beam (RPB). In recent years, the generation components for such beams were mainly focused on bulk devices, such as birefringent crystals[7] and spatial light modulators[8]. Recently, transversely dislocated fibers[9], tapered fibers[10], long period fiber gratings[11], and acoustic flexural waves[12] were employed to generate CVBs by coupling the fundamental Gaussian mode into the TE_{01} mode (APB) or TM_{01} mode (RPB)[13]. In these abovementioned schemes, CVBs are formed external to the cavity, and their temporal properties depend on the states of input laser.

On the other hand, pulsed fiber lasers have also drawn a great deal of research interest due to their compact structure, low cost, and high stability. The saturable absorber (SA) is the key element to generate *Q*-switched or mode-locked pulses, whose optical absorption decreases with the increase of light intensity. In the past several decades, the semiconductor SA mirror is the most common element to generate pulsed lasers[14]. However, it generally requires complex semiconductor fabrication technology, and its operating bandwidth is usually less than 100 nm. Recently, researchers have developed several new types of saturable absorption materials, such as carbon nanotubes[15,16], graphene[17–22], topological insulators[23–26], black phosphorus (BP)[27–29], bismuthene[30], and transition metal dichalcogenides[31–34]. Graphene and topological insulators usually exhibit a zero-bandgap structure, while transition metal dichalcogenides have a bandgap from 0.8 to 2.1 eV. By decreasing the thickness of the BP, the bandgap varies from 0.3 eV (bulk) to 1.5 eV (monolayer)[35], which can fill up the gap between large-bandgap transition metal dichalcogenides and zero-bandgap graphene. Few-layer BP nanosheets can be easily obtained from the bulk crystal by mechanical exfoliation[36] or liquid phase exfoliation[37] approaches. Nonetheless, phosphorus atoms tend to react with the water or oxygen atoms, and few-layer BP will be easily oxidized in the atmosphere[29], which has greatly limited its applications. Thus, it is imperative to develop a new approach to improve the stability of BP-based SAs.

Actually, CVBs and fiber lasers are two fascinating branches that were developed independently in the past decades. It is reasonable to combine these two researches and develop a new type of fiber laser capable of delivering CVBs[9,38–40]. Here, anti-oxidized BP nanosheets are obtained based on the liquid exfoliation approach, using aqueous poly(dimethyldiallyl ammonium chloride) (PDDA) as a dispersion fluid. Then, a film-type SA is formed by combining BP nanosheets with polyvinyl alcohol (PVA). Additionally, a transverse mode converter is used to excite TE_{01}/TM_{01} mode and a two-mode fiber Bragg grating (TMFBG) can further extract that, allowing the emission of switchable APB/RPB. By incorporating the BP SA and the transverse mode converter into the resonator, stable *Q*-switched CVBs can be obtained in an erbium-doped fiber laser.

The BP SA is the key element to realize *Q*-switched operation in the fiber laser. Here, BP nanosheets are prepared by the liquid exfoliation approach. First, 20 μL PDDA (Sigma-Aldrich, 20 wt. %) was added into 20 mL deionized water and then ultrasonic treated for 5 min at 5% power via a TU-650Y ultrasonicator. Second, 10 mg bulk-state BP was put into the prepared solution, and the mixture was ultrasonicated for 120 min at 80% power. Third, the dispersive solution was centrifuged at

the speed of 6,000 r/min for 10 min to remove the large-scale BP sediments by a Cence-H1850 centrifuger. After that, multi-layer PDDA-functionalized BP nanosheets could be obtained by further centrifuging the remaining solution at the speed of 11,000 r/min for 10 min.

We characterized the BP nanosheets by an atomic force microscope (AFM). As depicted in Fig. 1(a), the BP nanosheets possess a thickness of about 4 nm, indicating that we successfully prepared multi-layer BP. Besides, the Raman spectra of BP nanosheets after being exposed to air for 1 day and 15 days are shown in Fig. 1(b). There is no obvious difference in the distribution of the three typical peaks (A_g^1, B_{2g}, and A_g^2), which validates that the prepared BP nanosheets are anti-oxidized. This can be attributed to the electrostatic interactions between positive-charged nitrogen atoms of PDDA and lone-pair electrons in phosphorus atoms of BP that indeed help BP nanosheets absorb PDDA molecules[29].

Finally, the prepared aqueous BP nanosheets were blended with PVA solution to form a thin film by evaporating the mixture on a Petri dish. The side profile of the BP-PVA film is measured by a scanning electron microscope (SEM), which gives a thickness of 49.46 μm, as described in Fig. 1(c). The transmission versus illumination intensity of the film is recorded by a balanced twin-detector system[41]. The pulse used in the system is a Gaussian beam in the spatial domain, and it has a center wavelength of 1560 nm, a pulse duration of 654 fs, and a repetition rate of 15.52 MHz. As shown in Fig. 1(d), the transmission first increases with the pulse intensity and then becomes saturable, confirming that BP-PVA film can be used as an SA. Besides, we fit the data with the most common SA model[42], which can be expressed as follows:

$$T = 1 - \frac{\alpha_s}{1 + I/I_s} - \alpha_{\text{ns}},$$

where T is the transmission, α_s is modulation depth, α_{ns} is a component, I and I_s denote the input optical intensity and the saturable optical intensity, respectively.

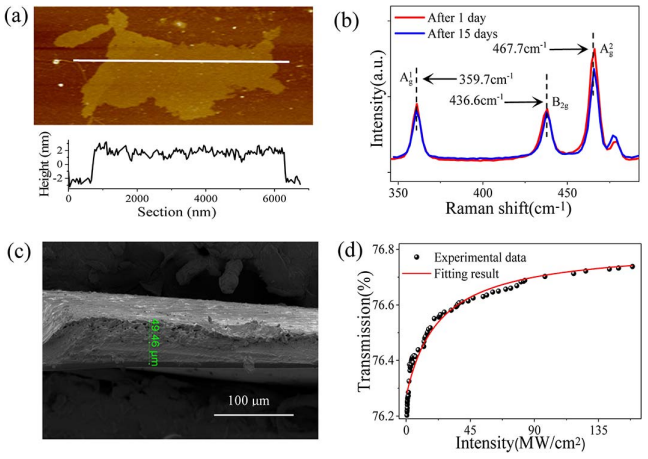

Fig. 1. (a) AFM image and (b) Raman spectra of BP nanosheets. (c) Side profile and (d) saturable absorption of BP-PVA film.

According to the fitting result, the saturable intensity and modulation depth of the BP-PVA film are about 23.5 MW/cm^2 and 0.53%. Moreover, we measured the transmission of the film after one month again, and we find there is negligible variation in the modulation depth, which further attests the high stability of the BP-PVA film.

To excite the CVBs in the fiber laser, a mode converter is manufactured by heating single-mode fiber (SMF, Corning SMF-28) and two-mode fiber (TMF, OFS, two-mode step-index fiber) with a CO_2 laser and then drawing them by a stepper motor. The length of the coupling region is about 2 mm, and the waist radius of the tapered fibers is about 7.6 μm. In the coupling zone, a portion of the fundamental Gaussian mode in the SMF is transferred to higher-order modes in TMF via the evanescent wave. When a light of 6.799 mW is input to the mode converter from the SMF terminal, the output power of another terminal is 6.168 mW, indicating the insertion loss of 0.42 dB. Meanwhile, a TMFBG placed after the mode converter is employed to extract the desired CVBs. Since the two modes in the TMF have different effective refractive indices, there are two peaks on the reflection spectrum of TMFBG, as shown in Fig. 2(a). Here, peak 1 at 1548.3 nm represents the coupling of the fundamental mode to the first group higher-order modes, while peak 2 at 1549.7 nm indicates that of fundamental mode to fundamental mode. If the laser wavelength locates at peak 2, the fundamental mode will be reflected back into the cavity, while higher-order modes can be exported from the TMFBG. Since the higher-order modes TE_{01} and TM_{01} correspond to APBs and RPBs, respectively, the mode

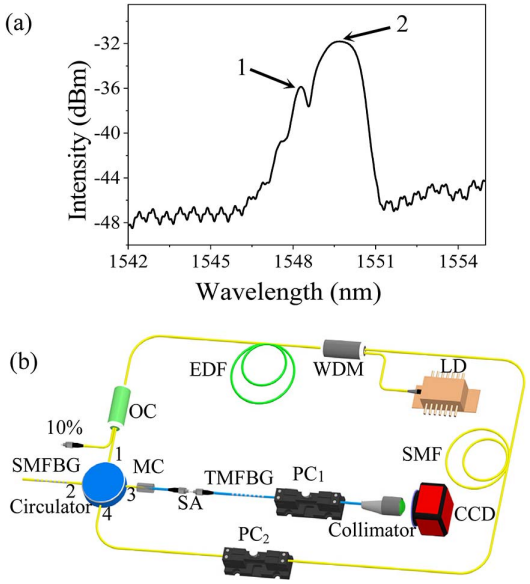

Fig. 2. (a) Reflection spectrum of the TMFBG. (b) Setup of BP Q-switched cylindrical vector laser. LD, laser diode; WDM, wavelength division multiplexer; EDF, erbium-doped fiber; OC, output coupler; SMFBG, single-mode fiber Bragg grating; MC, mode converter; SA, saturable absorber; TMFBG, two-mode fiber Bragg grating; PC, polarization controller; CCD, charge coupled device; SMF, single-mode fiber.

converter together with the TMFBG can excite and extract the APB/RPB.

Based on the aforementioned three elements, we have constructed an all-fiber BP Q-switched cylindrical vector laser, as illustrated in Fig. 2(b). In the proposed fiber laser, a 976 nm laser enters the cavity through the wavelength division multiplexer (WDM) and pumps a 6 m erbium-doped fiber (Nufern EDFL-980-HP). After that, 10% of the laser is output by an output coupler, and the residual laser comes into port 1 of the circulator. Then, the laser is reflected by a single-mode fiber Bragg grating (SMFBG) placed in port 2 and enters port 3. In port 3, part of the fundamental mode in the SMF couples into higher-order modes via a mode converter. The hybrid modes pass through the SA, and the higher-order modes are further extracted from the hybrid modes by the TMFBG. Simultaneously, the TMFBG reflects the fundamental mode back into port 4, and it will go into the WDM for the next circulation. The circulator forces the unidirectional propagation of the laser, while the SMFBG can fix the operation wavelength of the laser. The total optical length of the laser is 27.9 m. A collimator placed after the TMFBG expands the laser, and the spatial distribution is shot with a near-infrared charge coupled device (CCD). An optical spectrum analyzer (YOKOGAWA, AQ6370), a high-speed positive-intrinsic-negative (PIN) photodetector (PD 03), and a digital phosphor oscilloscope (Tektronix, DPO 3054) are utilized to measure the temporal properties of the Q-switched laser from the output coupler synchronously.

As the pump power reaches up to 64.68 mW, the proposed fiber laser evolves automatically from continuous-wave operation into Q-switched operation. By further adjusting the polarization controller before the mode converter, CVBs can be obtained from the two-mode collimator. It is worth noting that the operation is sensitive to the input polarization state in the SMF and can be switched between APB and RPB using the polarization controller. This is attributed to the continuous tangential electric field in the coupling zone of the transverse mode converter. The spatial intensity distribution of the RPB/APB at the pump of 79.85 mW is depicted in Figs. 3(a) and 3(b), which displays a doughnut-like profile with a dark spot in the center. To further distinguish RPB and APB, a linear polarizer is put between the two-mode collimator and CCD, whose transmission orientations are denoted by white arrows in Fig. 3. As shown in Figs. 3(a1)/3(b1) to 3(a4)/3(b4), after passing through the linear polarizer, the intensity profiles of APB/RPB are filtered into two parts with a dim band parallel/perpendicular to the transmission orientation of the linear polarizer.

We also record the corresponding output spectra and pulse trains of the Q-switched RPB/APB. As depicted in Fig. 3(c), the central wavelength and 3 dB bandwidth of Q-switched RPB/APB are 1549.5/1549.2 nm and 0.034/0.045 nm due to the wavelength filtering effect of the SMFBG, respectively. The APB and RPB possess different center wavelengths, which may result from their unequal effective refractive indices. The pulse interval and

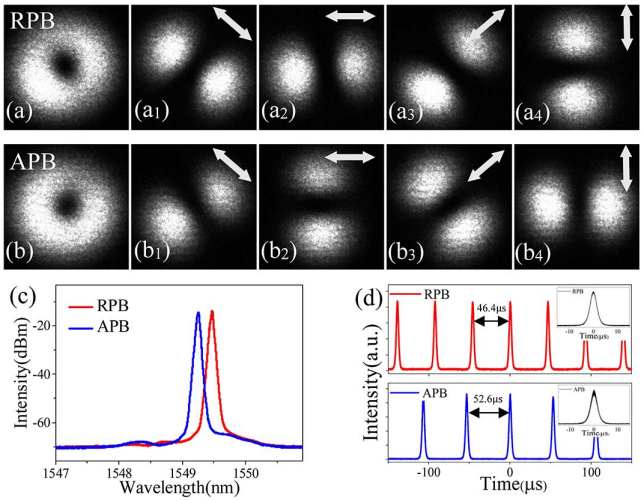

Fig. 3. Spatial intensity distributions of Q-switched (a) RPB and (b) APB, and their corresponding evolution with the rotation of the linear polarizer. (c) Optical spectra and (d) pulse trains of typical Q-switched APB and RPB at the pump power of 79.85 mW.

pulse duration of Q-switched RPB/APB are 46.4/52.6 μs and 3.34/3.32 μs, respectively. The fiber laser can stably emit Q-switched APB or RPB during the whole experiment (about 5 h), and the spectrum and pulse train stay almost unchanged at a fixed pump power. As the BP is polarization sensitive[35], it is hard to generate CVBs using a single piece of BP nanosheet as the SA. However, the proposed fiber laser successfully emits APB or RPB because the thickness of the BP-PVA film is hundreds of times that of BP nanosheets, which allows nanosheets being distributed in all orientations.

When the pump power varies between 64.68 and 174.82 mW, the fiber laser maintains a stable Q-switched operation. The pulse duration and repetition rate versus pump power are shown in Fig. 4(a). One can observe that the pulse duration of the Q-switched RPB/APB decreases from 4.23/4.44 μs to 1.77/1.73 μs, while the repetition rate enhances from 19.25/16.72 kHz to 37.82/30.71 kHz, exhibiting the typical characteristics of the Q-switched operation. The output powers of RPB/APB from the coupler and the two-mode collimator are recorded for comparison. As illustrated in Fig. 4(b), the output power of RPB/APB from the output coupler ranges from 0.51/0.43 mW to

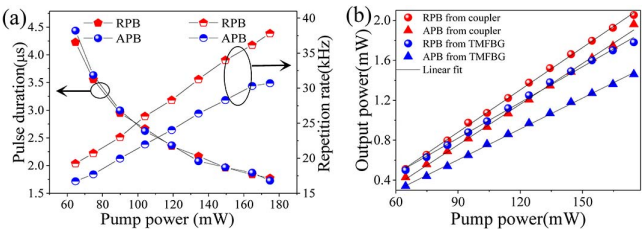

Fig. 4. (a) Repetition rate and pulse duration versus pump power. (b) Evolution of output power of RPB/APB from TMFBG and coupler with pump power (the linear fitting results are denoted by black lines).

2.50/1.96 mW, while that of RPB/APB from the two-mode collimator varies from 0.50/0.34 mW to 1.78/1.46 mW. The maximum pulse energy of *Q*-switched RPB/APB is 47.1/47.6 nJ. The output powers of the two operations are slightly different, which can be attributed to the polarization-dependent coupling efficiency of the mode converter. Considering that the output ratio of the output coupler is 10% and the transmission of the BP-PVA film is about 77%, we find that the highest coupling efficiency of converting the fundamental mode to radially and azimuthally polarized state is calculated as 12.7% and 10.6%, respectively. When the pump power is more than 180 mW, the *Q*-switched operation becomes unstable and finally unobtainable, no matter how we change the pump power or modulate the polarization controller, indicating that the SA has collapsed.

Finally, we remove the BP-PVA film from the fiber laser to study whether the *Q*-switched operation is purely induced by the film. The two-mode collimator can still export CVBs, however, the laser beam maintains continuous operation and *Q*-switched operation is not obtainable in any of the cases. This observation attests that BP-PVA film is the essential element to realize *Q*-switched operation. However, we have not observed mode-locked operation in the cylindrical vector laser, which can be attributed to the small modulation depth of the SA. By optimizing the layer number of BP to obtain SAs with higher modulation depths, mode-locked CVBs may be achieved in the fiber laser.

In conclusion, we propose an erbium-doped fiber laser to output *Q*-switched CVBs via BP-PVA film and a tapered mode converter. The BP-PVA film is employed as an SA to sharpen the pulse, while a transverse mode converter and a TMFBG are used to excite and extract RPB/APB. Moreover, the output CVBs are switchable between APBs and RPBs with a polarization controller. With the enhancement of pump power from 64.68 to 174.82 mW, the pulse duration of *Q*-switched RPB/APB varies from 4.23/4.44 μs to 1.77/1.73 μs, while the repetition rate of *Q*-switched RPB/APB ranges from 19.25/16.72 kHz to 37.82/30.71 kHz. Due to the unique temporal and spatial properties of *Q*-switched CVBs, as well as its flexibility and low cost, the fiber laser will be a great potential light source for fundamental researches and practical applications.

This work was supported by the National Key R&D Program of China (No. 2017YFA0303800) and the National Natural Science Foundation of China (Nos. 61575162, 11874300, 11634010, 61675169, and 61505165). We also thank the Analytical & Testing Center of Northwestern Polytechnical University for characterizing the nanoparticles.

References

1. Q. Zhan, Adv. Opt. Photon. **1**, 1 (2009).
2. R. Drevinskas, J. Zhang, M. Beresna, M. Gecevičius, A. G. Kazanskii, Y. P. Svirko, and P. G. Kazansky, Appl. Phys. Lett. **108**, 221107 (2016).
3. Q. Zhan, Opt. Express **12**, 3377 (2004).
4. G. M. Lerman, A. Yanai, and U. Levy, Nano. Lett. **9**, 2139 (2009).
5. A. Yanai and U. Levy, Opt. Express **17**, 924 (2009).
6. P. Zijlstra, J. W. Chon, and M. Gu, Nature **459**, 410 (2009).
7. K. Yonezawa, Y. Kozawa, and S. Sato, Opt. Lett. **31**, 2151 (2006).
8. M. Bashkansky, D. Park, and F. K. Fatemi, Opt. Express **18**, 212 (2010).
9. D. Mao, T. Feng, W. Zhang, H. Lu, Y. Jiang, P. Li, B. Jiang, Z. Sun, and J. Zhao, Appl. Phys. Lett. **110**, 021107 (2017).
10. D. Mao, Z. He, H. Lu, M. Li, W. Zhang, X. Cui, B. Jiang, and J. Zhao, Opt. Lett. **43**, 1590 (2018).
11. Y. Zhao, Y. Liu, L. Zhang, C. Zhang, J. Wen, and T. Wang, Opt. Express **24**, 6186 (2016).
12. W. Zhang, L. Huang, K. Wei, P. Li, B. Jiang, D. Mao, F. Gao, T. Mei, G. Zhang, and J. Zhao, Opt. Express **24**, 10376 (2016).
13. S. Ramachandran, P. Kristensen, and M. F. Yan, Opt. Lett. **34**, 2525 (2009).
14. D. H. Sutter, G. Steinmeyer, L. Gallmann, N. Matuschek, F. Morier-Genoud, and U. Keller, Opt. Lett. **24**, 631 (1999).
15. S. Y. Set, H. Yaguchi, Y. Tanaka, and M. Jablonski, IEEE J. Sel. Topics Quantum Electron. **10**, 137 (2004).
16. F. Wang, A. G. Rozhin, V. Scardaci, Z. Sun, F. Hennrich, I. H. White, W. I. Milne, and A. C. Ferrari, Nat. Nanotechnol. **3**, 738 (2008).
17. Q. Bao, H. Zhang, Y. Wang, Z. Ni, Y. Yan, Z. X. Shen, K. P. Loh, and D. Y. Tang, Adv. Funct. Mater. **19**, 3077 (2009).
18. Z. Sun, D. Popa, T. Hasan, F. Torrisi, F. Wang, E. J. R. Kelleher, J. C. Travers, V. Nicolosi, and A. C. Ferrari, Nano. Res. **3**, 653 (2010).
19. H. Zhang, D. Tang, R. J. Knize, L. Zhao, Q. Bao, and K. P. Loh, Appl. Phys. Lett. **96**, 111112 (2010).
20. N. Zhao, Z. Luo, H. Liu, M. Liu, X. Zheng, L. Liu, J. Liao, X. Wang, A. Luo, and W. Xu, IEEE Photon. Technol. Lett. **26**, 2450 (2014).
21. L. Li, X. Zheng, C. Jin, M. Qi, X. Chen, Z. Ren, J. Bai, and Z. Sun, Appl. Phys. Lett. **105**, 221103 (2014).
22. F. Zhao, Y. Wang, Y. Wang, H. Wang, and Y. Ca, Chin. Opt. Lett. **15**, 101402 (2017).
23. C. Zhao, H. Zhang, X. Qi, Y. Chen, Z. Wang, S. Wen, and D. Tang, Appl. Phys. Lett. **101**, 211106 (2012).
24. Z. C. Luo, M. Liu, H. Liu, X. W. Zheng, A. P. Luo, C. J. Zhao, H. Zhang, S. C. Wen, and W. C. Xu, Opt. Lett. **38**, 5212 (2013).
25. Y. Chen, C. Zhao, S. Chen, J. Du, P. Tang, G. Jiang, H. Zhang, S. Wen, and D. Tang, IEEE J. Sel. Topics Quantum Electron. **20**, 315 (2014).
26. X. Jiang, S. Liu, W. Liang, S. Luo, Z. He, Y. Ge, H. Wang, R. Cao, F. Zhang, Q. Wen, J. Li, Q. Bao, D. Fan, and H. Zhang, Laser Photon. Rev. **12**, 1700229 (2018).
27. H. Mu, S. Lin, Z. Wang, S. Xiao, P. Li, Y. Chen, H. Zhang, H. Bao, S. P. Lau, C. Pan, D. Fan, and Q. Bao, Adv. Opt. Mater. **3**, 1447 (2015).
28. Y. Chen, G. Jiang, S. Chen, Z. Guo, X. Yu, C. Zhao, H. Zhang, Q. Bao, S. Wen, D. Tang, and D. Fan, Opt. Express **23**, 12823 (2015).
29. Q. Feng, H. Liu, M. Zhu, J. Shang, D. Liu, X. Cui, D. Shen, L. Kou, D. Mao, J. Zheng, C. Li, J. Zhang, H. Xu, and J. Zhao, ACS Appl. Mater. Interfaces. **10**, 9679 (2018).
30. L. Lu, Z. Liang, L. Wu, Y. Chen, Y. Song, S. C. Dhanabalan, J. S. Ponraj, B. Dong, Y. Xiang, F. Xing, D. Fan, and H. Zhang, Laser Photon. Rev. **12**, 1700221 (2018).
31. H. Zhang, S. B. Lu, J. Zheng, J. Du, S. C. Wen, D. Y. Tang, and K. P. Loh, Opt. Express **22**, 7249 (2014).
32. Y. Huang, Z. Luo, Y. Li, M. Zhong, B. Xu, K. Che, H. Xu, Z. Cai, J. Peng, and J. Weng, Opt. Express **22**, 25258 (2014).
33. D. Mao, X. She, B. Du, D. Yang, W. Zhang, K. Song, X. Cui, B. Jiang, T. Peng, and J. Zhao, Sci. Rep. **6**, 23583 (2016).

34. D. Mao, X. Cui, X. Gan, M. Li, W. Zhang, H. Lu, and J. Zhao, IEEE J. Sel. Topics Quantum Electron. **24**, 1100406 (2018).
35. D. Li, H. Jussila, L. Karvonen, G. Ye, H. Lipsanen, X. Chen, and Z. Sun, Sci. Rep. **5**, 15899 (2015).
36. W. Tao, X. Zhu, X. Yu, X. Zeng, Q. Xiao, X. Zhang, X. Ji, X. Wang, J. Shi, H. Zhang, and L. Mei, Adv. Mater. **29**, 1603276 (2017).
37. D. Hanlon, C. Backes, E. Doherty, C. S. Cucinotta, N. C. Berner, C. Boland, K. Lee, A. Harvey, P. Lynch, Z. Gholamvand, S. Zhang, K. Wang, G. Moynihan, A. Pokle, Q. M. Ramasse, N. McEvoy, W. J. Blau, J. Wang, G. Abellan, F. Hauke, A. Hirsch, S. Sanvito, D. D. O'Regan, G. S. Duesberg, V. Nicolosi, and J. N. Coleman, Nat. Commun. **6**, 8563 (2015).
38. J. Lin, K. Yan, Y. Zhou, L. X. Xu, C. Gu, and Q. W. Zhan, Appl. Phys. Lett. **107**, 191108 (2015).
39. B. Huang, J. Yi, L. Du, G. Jiang, L. Miao, P. Tang, J. Liu, Y. Zou, H. Luo, C. Zhao, and S. Wen, IEEE J. Sel. Topics Quantum Electron. **23**, 26 (2017).
40. Z. Zhang, Y. Cai, J. Wang, H. Wan, and L. Zhang, IEEE J. Sel. Topics Quantum Electron. **24**, 1100906 (2018).
41. D. Mao, B. Du, D. Yang, S. Zhang, Y. Wang, W. Zhang, X. She, H. Cheng, H. Zeng, and J. Zhao, Small **12**, 1489 (2016).
42. S. B. Lu, L. L. Miao, Z. N. Guo, X. Qi, C. J. Zhao, H. Zhang, S. C. Wen, D. Y. Tang, and D. Y. Fan, Opt. Express **23**, 11183 (2015).